Microglial phenotypes in the human epileptic temporal lobe

Mélanie Morin-Brureau, Giampaolo Milior, Juliette Royer, Farah Chali, Caroline Le Duigou, Etienne Savary, Corinne Blugeon, Laurent Jourdren, David Akbar, Sophie Dupont, et al.

Published in final edited form as:
Brain. 2018 December 01; 141(12): 3343–3360. doi:10.1093/brain/awy276.

Microglial phenotypes in the human epileptic temporal lobe

Mélanie Morin-Brureau[1,*], **Giampaolo Milior**[1], **Juliette Royer**[1], **Farah Chali**[1], **Caroline LeDuigou**[1], **Etienne Savary**[1], **Corinne Blugeon**[2], **Laurent Jourdren**[2], **David Akbar**[1], **Sophie Dupont**[3], **Vincent Navarro**[3], **Michel Baulac**[3], **Franck Bielle**[3], **Bertrand Mathon**[3], **Stéphane Clemenceau**[3], and **Richard Miles**[1,*]

[1]Inserm U1127, CNRS UMR7225, Sorbonne Universités, UPMC Univ Paris 6 UMR S1127, Institut du Cerveau et de la Moelle épinière, Paris 75013, France

[2]École normale supérieure, PSL Research University, CNRS, Inserm, Institut de Biologie de l'École normale supérieure (IBENS), Plateforme Génomique, 75005 Paris, France

[3]AP-HP, GH Pitie-Salpêtrière-Charles Foix, Epilepsy Unit (VN, MB, SD), Neuropathologie (FB), Neurochirurgie (BM, SC), Paris 75013, France

Abstract

Microglia, immune cells of the brain, are highly plastic and possess multiple functional phenotypes. Differences in phenotype in different regions and different states of epileptic human brain have been little studied. Here we use transcriptomics, anatomy, imaging of living cells and ELISA measurements of cytokine release to examine microglia from patients with temporal lobe epilepsies. Two distinct microglial phenotypes were explored. First we asked how microglial phenotype differs between regions of high and low neuronal loss in the same brain. Secondly we asked how microglial phenotype is changed by a recent seizure. In sclerotic areas with few neurons, microglia have an amoeboid rather than ramified shape, express activation markers and respond faster to purinergic stimuli. The repairing interleukin, IL-10, regulates the basal phenotype of microglia in the CA1 and CA3 regions with neuronal loss and gliosis. To understand changes in phenotype induced by a seizure, we estimated the delay from the last seizure until tissue collection from changes in reads for immediate early gene transcripts. Pseudotime ordering of this data was validated by comparison with results from kainate-treated mice. It revealed a local and transient phenotype in which microglia secrete the human interleukin CXCL8, IL-1B and other cytokines. This secretory response is mediated in part via the NRLP3 inflammasome.

Keywords

Epilepsy; microglia; seizure; neuronal loss; cytokine

[*]Corresponding authors: melanie.morin@icm-institute.org; richard.miles@icm-institute.org, Institut du cerveau et de la moelle épinière, CHU Pitié-Salpêtrière, 47 bd de l'hôpital, Paris 75013.

None of the authors have competing interests.

Europe PMC Funders Author Manuscripts

Introduction

Inflammation is both a cause and consequence of epilepsy and immune signals in an epileptic brain have several origins. Some acquired epilepsies develop after brain infections (Popkirov et al., 2017) and auto-immune epilepsies result from antibodies generated against brain proteins (Irani et al., 2011). Inflammatory molecules facilitate epileptic activities (Vezzani et al., 2013; Chiavegato et al., 2014). Immune signals in an epileptic brain have several origins. Neuronal death induces a persistent immune response (Amor et al., 2014; Peruzzotti-Jametti et al., 2014). Furthermore, a seizure triggers a distinct immune reaction with secretion of inflammatory mediators (Vezzani et al., 1999; Ravizza et al., 2008).

Glial cells participate in both persistent reactions to neuronal damage and dynamic responses to high levels of neuronal firing or seizures. Of the two major glial cell types, the role of microglia, brain-resident immune cells, has been less well studied. Microglia are highly plastic cells which, in response to neuronal, immune and vascular signals among others, change phenotype to assume distinct functional roles. Among functions relevant to an epileptic brain, microglia secrete inflammatory molecules (Charolidi et al., 2015), extend processes towards damaged cells (Davalos et al., 2005), phagocytose debris (Koizumi et al., 2007) and also protect neurons from damage (Park et al., 2007).

Work in human epileptic tissue, obtained after operations to remove a focus (Crespel et al., 2002; Ravizza et al., 2008; Leal et al., 2017), has shown that microglia and astrocytes are activated and pro-inflammatory molecules are upregulated, as in rodents. However a more detailed study on immune cells and inflammation in human epilepsy is compelling for several reasons. First, recent data suggests human and rodent microglia may differ (Galatro et al., 2017; Boche et al., 2013). Second, there is little data comparing basal profiles of microglia in regions of neuronal loss and gliosis with those of microglia in other regions of an epileptic brain with lower neuronal loss. In tissue from patients with MTLE-HS, neuronal loss and gliosis are usually most severe in the CA1 or hilar regions and less pronounced in the subiculum (Blümcke et al., 2013). Third, data on immune responses to a seizure derives largely from convulsant applications to rodent brain resulting in a status epilepticus type of activity which may last for several hours (Vezzanni et al.; 1999; Ravizza et al; 2008; Avignone et al., 2015) compared to most human seizures. Indirect evidence for an immune response to a human seizure consists of higher levels of inflammatory markers in blood (Virta et al., 2002) and transcriptomic changes in immune molecules and cells in tissue from patients reporting high seizure frequencies (Pernhorst et al., 2013; Boer et al., 2006). Data on the delay between the last seizure and tissue collection is critical to specify the role of microglia in the response to a seizure.

Here we examine human tissue from patients with an intractable epileptic syndrome: mesial temporal lobe epilepsy with hippocampal sclerosis (MTLE-HS). We first compare basal phenotype, including shape, molecular markers and live responses to purinergic stimulation, for microglia in regions of greater or lesser neuronal loss in tissue from MTLE-HS patients. Transcriptomic data was derived from whole tissue of different regions, to minimize phenotypic changes due to cell isolation. It suggested the repair associated interleukin, IL10, was a critical regulator in the sclerotic CA1 and CA3 regions. The dynamic response to a

Europe PMC Funders Author Manuscripts

seizure was first examined by comparing transcriptomic data from tissue of patients reporting high or low seizure frequencies. Since few transcripts differed, we used reads for immediate early genes from each sample to estimate the delay from the last seizure until surgery. Ordering these delays revealed a fast, innate response including upregulation of the human cytokine CXCL8 and IL-1B. The involvement of specific cytokines was verified anatomically and was supported by ELISA analysis of secretion after seizure-like activity induced in acute human slices.

Materials and Methods

Epileptic patients

This study was performed on tissue obtained after operations on 25 patients (8 male, 17 female; 23–66 years) diagnosed with medial temporal lobe epilepsies associated with hippocampal sclerosis. Focal epileptic tissue was removed with minimal cauterization. All patients gave a written, informed consent. Protocols were approved by the Comité de protection des personnes, Ile-de-France (C16-16, 20152482). Supplementary Table 1 gives the gender and age of patients, the type of hippocampal sclerosis (Blümcke et al., 2013), estimates for seizure frequency and the delay between the last seizure and surgery and other clinical information.

Temporal lobe tissue from epileptic patients

Blocks of temporal lobe tissue including the CA1 and CA2/CA3 regions, dentate gyrus/hilus and subiculum (SUB) were transported in the following solution: sucrose, 248; $NaHCO_3$, 26; KCl, 1; $CaCl_2$, 1; $MgCl_2$, 10; glucose, 10 (mM; 4-8°C, 95% O_2/5% CO_2). Tissue from 13 patients, with information on seizure timing, was used for both transcriptome and anatomical analysis. For transcriptome analysis, the dentate gyrus/hilus, the CA2/3 and CA1 regions and SUB (Supplementary Fig.1) were separated and stored at -80 °C. For anatomy, 400µm thick slices were cut with a vibratome (HM650V, Microm), fixed with 4 % paraformaldehyde and stored at 4-8 °C. Tissue from 6 patients was used exclusively for anatomy. Tissue from 6 further patients was used for acute imaging and electrophysiology. Before recordings, 300-400 µm thick slices were stored at 20-24°C in: NaCl, 125; $NaHCO_3$, 26; KCl, 4; $CaCl_2$, 2; $MgCl_2$, 2; glucose, 10 (mM, 32-36°C, 95% O_2/5% CO_2).

Mouse model of epilepsy

Kainic acid (KA, 50 nl, 20 mM) or NaCl (50 nl, 0.9%) was stereotaxically injected into one hippocampus of mice anaesthetized with ketamine (80 mg/kg) and xylazine (12 mg/kg). Injections were made in the CA1 region (anterior-posterior, 1.8 mm; medial–lateral, 1.8 mm; dorsal-ventral, 1.8 mm from the bregma (70). Brains were removed and the CA1 region was microdissected (laser capture, PALM Microbeam, C Zeiss) from cryostat-cut (50 µm, CM1950, Leica) sections. RNA expression was measured for micro-dissected tissue at 6h, 1, 2, 4, 6 or 12 days after KA injection.

Immunostaining

Human tissue, cryoprotected in 30% sucrose, was kept at -80°C. Cryostat-cut sections (20 or 50 µm) were incubated in phosphate buffered saline (PBS) with bovine serum albumin

(BSA, 3%) and triton X100 (0.1-1%). They were immunostained by exposure to primary antibodies at 4°C overnight and then to secondary antibodies at 20-25 °C, for 2-3 hr.

Primary antibodies recognizing the following molecules were used: Cathepsin D (Santa-Cruz sc-10725; clone 1713, 1/50), CD68 (Dako clone KP1, 1/100), CD16/32 (Abcam 194937; clone 13D7, 1/100), CD163 (Biorad mca1853f, 1/50), FOSB (Abcam ab11959; 83B1138, 1/200), LAMP1 (Abcam ab25245, 1/200) MCH-II (Dako cloneCR3/43, 1/100), Iba-1 (Abcam ab5076; 1/500), CXCL8/IL-8 (Abcam ab18672, clone 807; 1/200), IL-10 (Abcam ab34843; 1/200), NeuN (Millipore MAB377, 1/500), SOCS3 (Abcam ab16030, 1/200), PYCARD/ASC (Adipogen AG 25B-006-C100, 1/100), NLRP3 (Adipogen AG-20B-0014-C100, clone Cry2, 1/200), P2Y12 (Novusbio NBP2-33870,1/200). Secondary antibodies were donkey anti-goat (Life technologies A488; 1/500) and donkey anti-mouse (Life technologies A555; A647; 1/500). Heat-induced antigen retrieval (citrate buffer, 95°C, pH=6) was used for CD68, MHCII and CD163. Nuclei were stained with DAPI. FOSB and CXCL8 were detected with a fluorescein amplification Kit (Perkin-Elmer). Slices were incubated in 1% triton X-100, in 3% H_2O_2 for 30 m and TNB buffer for 30 m, before exposure to FOSB or CXCL8 antibody in TNB (48 hr, 4°C). Slices were then exposed to donkey anti-mouse HRP (2 hr) before streptavidin (30 m) and fluorescein (10 m) to reveal FOSB or CXCL8.

Diaminobenzidine was used as a chromogen in immunostaining for other antibodies. 3 μm sections were cut from formalin-fixed, paraffin-embedded tissue and immunolabeling performed by an automated system (5Ventana benchmark XT, Roche) with hematoxylin-eosin counterstaining. Primary antibodies recognizing PTGS2 (COX2, 1/300, polyclonal rabbit, Cayman Chemical) and, GFAP (Millipore AB5804, 1/500) were revealed with the streptavidin–peroxidase complex with diaminobenzidine as chromogen.

Image acquisition and cell counting

Microglia and neuron density was measured automatically from 50 μm tissue sections immunostained for IBA1 and NeuN (Supplementary Fig.1D). Other immunostaining data was derived from stacks of 10-50 images at 0.5-1.0 μm z-interval made from 20 μm slices with an inverted Olympus IX81 microscope using an Optigrid II (Thales Optem, Qioptik) and a Retiga EXI camera (Qimaging). Pixel sizes were 0.16μm/pixel for a x40 and 0.32 μm/pixel for a x20 objective. Images were 1392*1040 pixels. Binarisation was not used. Co-localization of CXCL8, PYCARD and IBA1 was detected with Image J macros. PTGS2 immunopositive cells were visualized with a scanner (Nanozoomer, Hamamatsu).

RNAseq

RNA quantity (Nanodrop 1000, Thermo-Fisher) and RNA integrity number (RIN, Agilent 6000 Nano kit, Agilent Bioanalyzer 2100) were measured after extraction (Nucleospin XS kit, mouse; Nucleospin, human; Machery-Nagel). For human samples, the mean RIN number was 6.5 ± 1.0 (n=44) and for mouse samples 7.0 ± 0.5 (n=36). Samples were excluded when RIN quantity or integrity values were low. Libraries were made and sequencing performed at the Ecole Normale Supérieure Genomic Platform. For human samples, messenger (polyA+) RNAs were purified from ~300 ng of total RNA with oligo

(dT). Libraries were prepared with a strand specific RNA kit (TruSeq Stranded mRNA kit, Illumina) and multiplexed on flowcell lanes. 50 bp read sequencing was performed on a HiSeq 1500 device (Illumina). For mouse, 10 ng of total RNA was amplified and converted to cDNA (SMART-Seq v4 Ultra Low Input RNA kit, Clontech). Libraries were made from ~180 ng of amplified cDNA (Nextera XT DNA kit, Illumina) and multiplexed on flowcell lanes. 75 bp read sequencing was performed on a NextSeq 500 device (Illumina). The mean number of passing human filter reads was 59 ± 5 million (n=44) and for mouse tissue it was 80 ± 8 million (n=36).

Read filtering, mapping, alignment filtering, quantification, normalisation and differential analysis, were done with the Eoulsan pipeline (Jourdren et al., 2012). Before mapping, poly N read tails were trimmed, and reads with <40 bases or mean quality of <30 removed with SAMtools, Java (Li et al., 2009). Reads for human RNA were aligned against the hg19 annotated human genome (STAR, v2.4.0k). Mouse RNA reads were aligned to the mm10 mouse genome (Ensembl 81). Overlapping regions between alignments and referenced exons, or genes, were counted with HTSeq-count (v0.5.3).

Sample counts were normalized and transcript expression analysed with DESeq2 (v1.8.1; Love et al., 2014). This package uses a negative binomial model to control count variability and the Benjamini and Hochberg correction for multiple comparisons. Defaults were <0.05 for the adjusted p-value and 0.1 for the false discovery rate. We searched for differential transcript expression in several contexts: (a) basal profiles of regions with different degrees of neuronal death, (b) profiles of tissue from patients reporting high or low seizure frequencies; (c) dynamic profile of KA- and NaCl-treated mice at different delays. (d) in comparisons of each single human tissue sample with all other samples (all regions, all patients) to examine possible region-specific effects of a seizure. Supplementary material 4 describes the procedure for this comparison.

Ontology, pathways and cell type specificity of RNA species

Ingenuity pathway analysis (IPA, Qiagen) used differentially expressed transcripts in an experimental data set to derive enriched cellular functions and to predict upstream regulators such as cytokines. Statistical significance (p-overlap) of predictions was determined by comparing the number of differentially expressed transcripts in an experimental data-set with the total number of transcripts linked to a function or regulator. Z-scores were derived from agreement between the direction of predicted changes (up- or down-) and those present in the data set. Supplementary material 2 describes the construction and validation of a list of microglia-enriched transcripts (Kuhn et al., 2011). Supplementary Material 4 describes procedures for pseudo-time analysis and Supplementary Tables 3-6 list all differential transcripts together with enriched functions and predicted regulators.

Imaging microglia in tissue slices

Living microglia were labelled with tomato lectin conjugated to a fluorescent marker (Dy-light 594, Vector Labs; Schwendele et al., 2012). It was injected from glass micropipettes (50 μg/ml) to label cells at depths of 70-150 μm in 300 μm thick slices. Images were captured using a Zeiss Axio Z1 microscope with two-photon illumination (3i Intelligent

Imaging) from a Ti-sapphire laser (Chameleon, Coherent). The lectin was excited at 800 nm and emission measured at 620 nm. Objectives were 20x, NA 1.0 or 40x NA 1.0. ADP (2 mM) was applied in the ACSF bath perfusing solution.

Microglial motility and mobility were monitored from z-stacks of 30-40 μm at 0.5-1 μm collected at interval ~2m and analyzed with Slidebook software (3i Intelligent Imaging). Microglial shape was reconstructed and kinetic behaviours analysed from z-stacks. Changes in microglia form were analyzed by subtracting pairs of sequential images, to resolve changes in somatic area, process extension or retraction and membrane ruffling. Sidebook tools 'freehand selection' and 'polygon selection' were used to measure somatic area and arborization area for single cells. A morphological index was defined as the arborization area divided by the soma area. Bleb area was defined from lines drawn around extruded membrane.

ELISA measurement of cytokine release

Cytokine release was measured with an ELISA kit (human multi-analyte ELISA, Qiagen) for IL-1A, IL-1B, IL-2, IL-4, IL-6, CXCL8 (IL-8), IL-10, IL-12, IL-17A, IFNG, TNFA and GM-CSF. We tested supernatant collected over 2 hr from slices in an interface chamber at 32-35 °C, equilibrated with 95% O_2 / 5% CO_2. Seizure-like activity was induced in temporal lobe slices in an interface recording chamber by exposure to a solution containing NaCl, 125; $NaHCO_3$, 26; KCl, 8-10; $CaCl_2$, 2; $MgCl_2$, 0.1; glucose, 10 (in mM) equilibrated with 95% O_2/5% CO_2 at 34-36 °C. Epileptiform activity monitored with tungsten electrodes was amplified (3600, AM Systems) and digitized to a PC (Digidata 1200A, Molecular Devices).

Statistics

Variance is stated as standard error on the mean unless noted. Microglial shape parameters (Fig. 1) were compared with the Spearman correlation test and significance tested with the Kruskal-Wallis test. Changes in microglial shape during live records (Fig. 3) were assessed with unpaired t-tests and correlation linearity tested with the Pearson r coefficient. Analyses including histograms and heat-maps were made with GraphPad Prism. Unsupervised cluster analysis based on Euclidean distances using Ward's procedure was executed from the site http://biit.cs.ut.ee/clustvis/). Enrichment of pathways and functions was assessed with the hyper-geometric test (https://www.geneprof.org/GeneProf/tools/hypergeometric.jsp).

Data availability

RNASeq data are stored at the Gene Expression Omnibus (NCBI; human data, accession number: GSE94744; mouse data, GSE99577).

https://www.ncbi.nlm.nih.gov/geo/query/acc.cgi?token=gdahkeuqlxadrov&acc=GSE94744

Supplementary material is available at Brain online on: Human epileptic tissue: patients, tissue preparation, counting and characterizing cells. Data analysis strategies including extraction and verification of microglia specific transcripts. Transcriptomic data and analysis on regions of high or low neuronal loss and seizure frequency. Procedures to compare RNA expression in one sample versus many control samples.

Other aspects of data presented here will be shared on reasonable request.

Results

Microglia: shape

The human epileptic temporal lobe (MLTE-HS) includes the sclerotic CA1 and CA3 zones, where many neurons have died, the dentate gyrus (DG) and the subiculum (SUB) where fewer neurons have been lost and seizures may be initiated (Huberfeld et al., 2011). How does microglial phenotype vary in these regions? As a first element of their phenotype, we measured the shape of IBA1-immunopositive cells (n=283, 9 patients). Even for cells of the same region, shape varied considerably, (Fig. 1A). While both microglia and macrophages express IBA1, we found that IBA1+ cells of all shapes co-expressed P2RY12 (Supplementary Fig.1A, B), which is specific to rodent and human microglia (Mildner et al., 2014). Microglial shape was classified by a cluster analysis of indices to measure their somata and processes (Fig. 1B).

Canonical cells of these clusters ranged from highly ramified cells (cluster B2) to amoeboid cells with few processes (cluster A1), typical of activated microglia (Beach et al., 1995; Kettenmann et al., 2011). Clusters discriminated between different numbers of primary or secondary ramifications (Supplementary Fig.2). Microglia with shapes corresponding to each cluster were found in each region (Fig. 1C). Microglia with multiple secondary ramifications were most frequently situated in the SUB (70% of cells in cluster B1, 2) or the DG (50% of cells in clusters B1, 2). Those with few ramifications were found most often in CA1 and CA3 (60-70 % of cells in clusters A1, 2).

We asked whether different microglial shapes were correlated with local neuronal (Fig. 1D) or microglial density (Fig. 1E) in the CA2/CA3, CA1, SUB and DG/hilus regions. Mean neuronal density was consistently lower in the CA1 and CA3 regions (Fig. 1D), except for tissue from one patient with a distinct, type 3, pattern of sclerosis (Blümcke et al., 2013 defines 3 types of hippocampal sclerosis according to neuronal loss in the CA3 region and the hilus). Mean microglial density did not differ greatly between regions (Fig. 1E). Microglial and neuronal density were well correlated in CA1 and CA2/CA3 (Fig. 1F) but poorly correlated in the DG and SUB (Fig. 1G). In regions of low neuronal density, amoeboid cells (cluster A1) occurred more often, and ramified cells (cluster B1) less frequently (Fig. 1H). Microglial density and shape were not influenced by age or seizure frequency (Supplementary Fig.3A, B).

These data show a strong, but not absolute, segregation of microglia according to shape. Amoeboid microglia were most frequent in the sclerotic CA1 and CA3 regions accompanied by neuronal loss and astrocyte proliferation (Supplementary Fig.3G, H). Microglial density in these regions is correlated with neuronal density. Microglia of the DG tend to an intermediate shape with few processes while subicular microglia usually possessed multiple processes. Neuronal and microglial density were poorly correlated in the DG and subiculum.

Microglia: molecular markers

We next examined markers associated with different functional microglial phenotypes. Reactive microglia express proteins of the major histocompatibility complex type II (MHCII). Immunostaining against MHCII revealed punctate labelling in the soma and processes of some IBA1+ microglia (Fig. 2A). The form of MHCII+ cells, typically with simple ramifications, was significantly associated with clusters A1 and A2 (75%), and rather than B1 (60%) or B2 (30%) (Fig. 2B). These cells (Fig. 2C) were located more often in the CA1 (78%) and CA3 regions (82%) than in the DG (68%) or SUB (32%).

Markers of phagocytotic microglia include the glycoprotein CD68 and the immunoglobulin Fc receptor CD16/32a. CD68+ elements of diameter 2-5 μm were present in the processes of some moderately ramified microglia (Fig. 2D). Co-localization of CD68 staining with that for the glycoprotein Lamp1, and the protease cathepsin D (Fig. 2G) identified CD68+ elements as phagosomes or lysosomes. Immunopositivity for the Fc receptor CD32a, confirmed the phagocytic phenotype of some microglia (Fig. 2H). Cells expressing CD68 were not exclusively amoeboid but typically possessed moderate ramifications (Fig. 2E) and were detected in all regions (Fig. 2F).

Microglia: dynamic responses to purinergic agonists

As a third element of microglial phenotype, we asked whether purinergic stimuli had different effects on amoeboid and ramified cells. Purines are liberated during a seizure (Kumaria et al, 2008). Processes of healthy rodent microglia extend in response to purinergic stimuli (Davalos et al., 2005), but ‘activated’ microglia in an inflamed brain retract their processes (Gyoneva et al., 2014). We labelled microglia in acute tissue slices from MTLE-HS patients with a fluorescent tomato lectin (Schwendele et al., 2012) to compare the motility of amoeboid and ramified microglia using two photon microscopy.

We examine effects of ADP on amoeboid cells of the CA1 region and ramified microglia from SUB. Before purinergic stimulation, amoeboid cells were largely static, while processes of ramified microglia moved continuously. ADP (2 mM, 30 min) induced responses with distinct kinetics in amoeboid (n=7, 3 patients) and ramified (n=7, 3 patients) microglia (Fig. 3A, B). In amoeboid microglia, any short processes were retracted and somatic area increased over 5-15 min (Fig. 3C). Processes of ramified cells retracted partially over 9-15 min (Fig. 3B, D, yellow arrow). Ruffling was detected as a continuous extrusion and retraction of membrane from amoeboid cells or from the soma and processes of ramified microglia (Fig. 3A, B, blue). The latency to ruffling was significantly longer in ramified than in amoeboid microglia (Fig. 3E). It was well correlated with their morphological index, the perimeter area of the tips of all processes divided by somatic area (Fig. 3F). Microglial process retraction in response to ADP contrasts to the extension induced in healthy rodent cells.

Up-regulation of IL-10 signaling in regions of high neuronal loss

These data show that while microglia were heterogenous, those of sclerotic and less sclerotic regions tend to differ in shape, markers and response to purines. Are these differences correlated with a distinct transcriptomic profile? We used RNAseq to analyze whole tissue

from different regions thus minimizing potential phenotype changes during purification (Réu et al., 2017) and retaining links to the regional microenvironment. Our analysis strategy is described in Supplementary material 2. Since whole tissue RNA transcripts cannot be attributed to a specific cell-type, we constructed a list of microglia-enriched transcripts using a procedure based on seeding with microglia-specific transcripts (Kuhn et al, 2011). The identity of differentially regulated transcripts let us define enriched cellular processes and predict uptream regulators including cytokines and transcription factors. Immunostaining tissue from the same blocks used for transcriptomics let us examine cell-type specific expression of proteins corresponding to differentially expressed transcripts or regulators.

Since microglia of the DG were intermediate in shape (Fig. 1C) and marker expression (Fig. 2C), we compared RNA-seq data from the sclerotic CA1 and CA2/CA3 regions with that from SUB (n=12 patients). Fig. 4A shows a Venn diagram of differential expressed in the sclerotic CA1 and CA3 regions compared to subiculum (n=4014; p-adj <0.05; 149 with log FC >2). Analysis of cellular functions suggests common transcripts are associated with ‘activation’, ‘proliferation’ and ‘differentiation’ (Fig. 4B). Comparison with the cell-type specific list showed that 169 of 4014 transcripts were linked to microglia (Fig. 4A, Supplementary material 2). Enriched functions derived from the identity of these transcripts (Fig. 4C) were ‘activation’, ‘differentiation’, ‘migration’ and ‘inflammatory response’. ‘Phagocytosis’ was not enriched when data from the CA1 and CA2/CA3 regions was compared to that from SUB conforming to the presence of CD68+ microglia in both zones (Fig. 2F).

The 169 microglia related transcripts was then used to predict cytokine regulators of differences between sclerotic and less sclerotic regions. This procedure suggested IL-10, an anti-inflammatory cytokine (Saraiva and O’Garra, 2010), was associated with transcripts upregulated in the CA1 and CA2/3 regions. Actions of IL-10 tend to oppose those of Interferon gamma, IFNG, a cytokine associated with the classical activated microglial phenotype. Fig. 4D shows reciprocal actions of IL-10 and IFNG on transcripts up-regulated in regions with few neurons. They included the cytokines *CXCR4* and *CCR5,* involved in cellular migration, proliferation and also neuronal survival (Louboutin and Strayer, 2013; Nash and Meucci, 2014). Fig. 4E summarizes differential expression of transcripts coding for immune receptors (blue), transcription factors (green), and secreted molecules (purple) in the the CA1 and CA2/3 regions compared to SUB.

Transcriptional regulators predicted from differentially expressed transcripts suggest that IL-10 may also be coupled to vascular genesis in regions of neuronal death. They included EPAS1/HIF2A and KLF2, which control the transcripts *VCAM1* and *ANGPT2* linked to ‘angiogenesis’, ‘control of vascular morphology’ and ‘endothelial cell migration’. This prediction is consistent with angiogenesis described in tissue from MTLE-HS patients (Rigau et al., 2007).

To verify these predictions, immunostaining was used to compare expression of IL-10 and its targets in regions of high or low neuronal loss. IL-10 was strongly expressed in IBA1+, CD68+ cells of the CA1 region, but low in SUB. Some IL-10+ cells in CA1, clustered near blood vessels, may correspond to infiltrating macrophages (Fig. 4 F). CD163, an upregulated

target of IL-10, was also expressed in IBA1+ cells near blood vessels in CA1 but not in SUB (Fig. 4 G). IL-10 also induces SOCS3 which suppresses cytokine signaling (Carow and Rottenberg, 2014). SOCS3 was detected in both ramified and amoeboid IBA1+ cells in CA1, but was largely absent in IBA1+ cells of SUB (Fig. 4 H). These data suggest the phenotype of microglia in regions with few surviving neurons is linked to IL-10 and favours neuronal survival and angiogenesis.

Differential expression after recent seizure activity

We next asked how a seizure changes microglial phenotype. First we compared the transcriptomic profile of tissue from patients reporting a high or low seizure frequency. A threshold of 7 seizures per month separated 6 patients with high and 6 with low frequencies (Supplementary Table 1). Few transcripts were differentially expressed. In a region-by-region comparison, 47 transcripts were up- and 44 down-regulated (CA1, CA3, DG and SUB; p-adj <0.05 and log-FC >2). Four coding transcripts were common to more than 1 region. Relaxing the log-FC threshold (p-adj <0.05; Supplementary Fig.7) revealed up-regulation of transcripts associated with inflammation in tissue from patients reporting a high frequency.

It seemed paradoxical to find weak transcriptomic differences between tissue associated with high or low seizure frequencies (Pernhorst et al., 2013) when a strong immune response occurs after a seizure in animals (Lerner-Natoli et al, 2000). Several explanations are possible. A human seizure may have lesser effects than those of prolonged convulsant application in rodents. Reported frequencies may be unreliable if some seizures are not perceived (Cook et al., 2013). A seizure may have occurred just before tissue was obtained from a patient reporting a low frequency. We followed two strategies. First, we sought information on the delay between the last seizure and operation (Supplementary table 1). Second, we examined RNA-seq data for evidence of a recent seizure. Supplementary material 4 describes how we searched for differentially expressed transcripts in comparisons of each region of each sample (n=1) with all other samples (n=43; p-adj <0.05, log-FC> ±1.5).

This procedure resulted in 44 sets of differentially expressed transcripts. Next we attempted to sort them into a pseudo-time order (Trapnell et al., 2014) of delay from a seizure. Reads for immediate early gene transcripts were used as a surrogate molecular clock to measure time elapsed since recent, strong neuronal activity (Ryan et al., 2011; Lacar et al., 2017). We used the mean of reads for 10 transcripts: *ARC, EGR1, FOS, FOSB, FOSL1, IER2, JUN, JUNB, NR4A1* and *NR4A3*. To validate this approach, we examined changes in the same transcripts after kainic acid injection in the mouse, where delay after a seizure can be accurately measured. Fig. 5A shows mean normalized reads from human tissue sorted to a pseudo-time (ptime) order. Data for the same transcripts in the CA1 region of mouse hippocampus collected at 6 hrs -12 d after kainate injection is shown in Fig. 5B.

Immediate early gene transcripts were highly up-regulated in some, but not all, samples of one patient, strongly upregulated in some samples from three other patients and down-regulated for all others. In ptime1 tissue, from the patient with the shortest predicted delay from a seizure to tissue collection, reads were high in SUB, increased to a lesser extent in

Europe PMC Funders Author Manuscripts

CA2/CA3 but not in CA1 or DG samples (Fig. 5C; Supplementary Fig.9). In ptime2 tissue, reads were high in DG and CA2/CA3, but not CA1 or SUB samples. Immediate early gene reads were low in all regions at late ptime points. For each patient, the region with the highest mean reads for the immediate early genes was identified as the seizure associated area (Fig. 5C; Supplementary Fig.9).

Predictions of a recent, local seizure in some samples were tested by immunostaining for PTGS2, the prostaglandin synthetic enzyme, upregulated after a seizure, and for FOSB, an immediate early gene. Neuronal immunostaining for PTGS2 was restricted to seizure associated areas of tissue from short ptimes (Fig. 5D). FOSB staining was also detected in predicted seizure-associated regions at ptime1, but was absent from all areas at ptime4 (Fig. 5E).

Pseudotime ordering let us examine the time course of microglial activation after a seizure (Fig. 5Fi-iv). Analysis of differentially expressed transcripts for each sample with all other samples (1vs43) showed the function ‘epileptic activity’ was enriched in some, but not all regions, of samples from ptimes1-8 (Fig. 5Fi; Supplementary material 4). Immediate early genes were upregulated, in the same regions at ptimes1-4 (Fig. 5Fii). The kinetics of microglial activation (Fig. 5Fiii), derived from enrichment of transcripts of the microglia-filtered list (Supplementary Table 2), followed a similar pattern to that of immediate early genes. In seizure-related regions at ptimes 1-4, we detected an increase in microglia of amoeboid shapes with few processes (clusters A1, 2) and an increase in their expression of MHC II (Supplementary Fig.3). Fig. 5Fiv confronts transcriptomic evidence with data from patients. Of four patients with the shortest estimated ptimes, two reported a high, and two a low seizure frequency. Two of these patients reported a seizure in the 4 days before tissue collection (Supplementary Table 1). For further analysis, data were separated into three groups: early ptimes (1-4), mid ptimes (5-9) and late ptimes (10-13).

Local microglial response to a seizure

This procedure let us identify transcripts up-regulated in seizure-related regions at short ptimes (log_2-fold change> ±1.5, p-adj<0.05; Supplementary material 4). They included cytokines (Fig. 6A), transcription factors (Fig. 6B) and other elements of an immune response (Fig. 6C) while the great majority of transcripts were not changed (insets Fig. 6A-C). Highly up-regulated cytokines at ptimes1-4 included the human inflammatory cytokine *CXCL8,* as well as the pro-inflammatory *IL-6, IL-1B*, *CCL3* and the regulatory cytokine *OSM* (Fig. 6A). Up-regulated transcription factors included *REL,* an element of the NFKB family, *MAFF*, *KLF4, NFKBIZ,* a negative control of NFKB pathways and *NR4A2,* which inhibits production of inflammatory mediators (Fig. 6B). Other transcripts upregulated at short ptimes included *PTGS2*, a synthetic enzyme of prostaglandins, *GADD45B*, *SERPINE1*, *BCL2A1*, a pro-apoptotic target of NFKB, and *NLRP3*, a component of the inflammasome (Fig. 6C). As for immediate early gene transcripts (Fig. 5C, Fii), up-regulation of those coding for cytokines and transcription factors was local. It was restricted to one or two regions of the same tissue sample from ptimes1-4 (Supplementary Fig.10).

These conclusions depend on transcriptomic data from few patients. In order to validate them, we compared the identity of upregulated cytokine transcripts with that of cytokines

secreted from MTLE-HS tissue slices after the induction of seizure-like activity (Fig. 6D-E). Slices from patients with unknown seizure history were used (n=6). Seizure-like activity was induced with a high –excitability solution (8-10 mM K, 0.1 mM Mg; 30-60 min). Cytokine secretion was measured by multiplex ELISA on supernatant collected during 2 hours after induced seizures, compared to control slices with no induced seizures. The most highly secreted cytokine was the interleukin CXCL8 (Fig. 6E). Significant increases were also detected for IL-1A>IL-1B>IL-6>TNFA (n=6). Fig. 6F shows upregulation of transcripts coding for these cytokines in seizure-related areas at ptime1 (*CXCL8>IL-1A>IL-1B>IL-6>TNFA*). Comparing the rank order of changes in reads to ELISA data on secretion gave a p-value of 0.0003. The anti-inflammatory cytokine IL-10 was not secreted. These data suggest that secreted cytokines conform to those with increased mRNA levels after a seizure.

We pursued this point by immunostaining for CXCL8 protein in the same tissue as used for transcriptomic analysis. CXCL8 was detected in the soma and processes of most microglia at all ptimes (Fig. 6G, purple) including both ramified (clusters B1, 2) and amoeboid (clusters A1, 2) IBA1+ cells. In seizure-associated regions at ptimes1-4, CXCL8+ staining was detected both inside microglia (Fig. 6H, white arrows) and extracellularly (Fig. 6H, yellow arrows). On average, 18 CXCL8+ elements of diameter 1-2 μm were detected near each microglia. These data point to a local and transient secretion of CXCL8.

The NLRP3 inflammasome in the microglial response to a seizure

Our data suggest the inflammatory cytokine IL-1B is also secreted after a seizure. Transcripts selectively upregulated in seizure associated areas at ptimes1-4 (Fig. 7A, B) predict secretion may involve the NLRP3 inflammasome, a multi-molecular complex which processes some cytokines for release (Latz et al., 2013). Predicted regulators linked to the inflammasome included *NLRP3, PYCARD* and *CASP1* (Fig. 7A, B). NLRP3 is a sensor molecule that may be activated by purines acting at the P2RX7 receptor (Franceschini et al., 2015; Jimenez-Pacheco et al 2016). Transcripts for *NLRP3, CASP1, IL1B, CCL2* and *CXCL8* were all upregulated at ptimes1-4 (Fig. 7B).

We therefore asked whether purinergic stimuli induced secretion of a similar spectrum of cytokines to those up-regulated after seizure-like activity. Release was again measured by multiplex ELISA on supernatant collected over 2 hrs after exposure of acute tissue slices from MTLE-HS patients to ADP (2mM, 30 min; n=4). While cytokine secretion induced by ADP was less than that induced by seizure like activity, IL-1B, CXCL8, IL-6 and TNFA were detected at levels higher than control (n=4; Fig. 7C).

We attempted to confirm these predictions by immunostaining for NLRP3 and PYCARD in tissue from the blocks used for transcriptomic analysis. At ptimes1-4, discrete aggregates of NLRP3 (white arrow, Fig. 7D) were apparent in 20-25% of microglia, particularly amoeboid cells. Confirming the transient increase in NLRP3 message from RNA-seq data, NLRP3 immunopositivity was not observed at later ptimes (Fig. 7E, F). In contrast, PYCARD signals were detected in most IBA1+ microglia (95%) at all ptimes in accord with transcriptomic data (Fig. 7G). PYCARD co-localized with NLRP3 in somatic regions of 20% of IBA1+ cells at ptimes1-4 (Fig. 7H, blue arrow). However PYCARD signals,

detected in 60% of microglia at later ptimes, were diffusely distributed throughout cellular processes (Fig. 7H, blue arrow). This intracellular redistribution of PYCARD (Bryan et al, 2009) is consistent with a transient, perisomatic assembly (Fig. 7I) of the NLRP3 inflammasome for cytokine secretion.

Discussion

This data defines two distinct phenotypes for microglia of human, epileptic temporal lobe. Cells in regions of intense neuronal loss tend to an amoeboid shape in contrast to a ramified form for those in regions with more surviving neurons. The anti-inflammatory cytokine IL-10 is a key influence on the phenotype of microglia in sclerotic regions. The second phenotype occurs transiently after a seizure. The secretion of inflammatory molecules including the human interleukin CXCL8 and IL-1B by microglia in a local region is mediated in part by the NRLP3 inflammasome.

Experimental design

We note several aspects of our approach. First, we analyzed whole tissue from different regions of epileptic brain rather than purified microglia. While sorting removes doubts on cell-specificity, whole-tissue analysis minimizes changes in phenotype (Réu et al., 2017; Bohlen et al, 2017) and cell loss (Galatro, et al., 2017) during separation. Transcripts enriched in microglia were extracted with an analysis based on seeding with cell specific transcripts (Kuhn et al., 2011).

Second, the kinetic response to a seizure was examined using a pseudotime sorting procedure. Reads for immediate early genes were used to estimate the time between the last seizure and tissue collection. Immediate early genes are transiently activated by strong neuronal activity, so this approach was possible in whole tissue. Predicted kinetics of the response to a seizure were verified in several ways. Firstly, by comparison with changes in the same transcripts in mouse tissue at known delays after an induced seizure. Secondly, from local expression of the early gene FOSB and PTGS2, in tissue where a recent seizure was predicted. Finally predictions on cytokine secretion were validated by comparing the identity of up-regulated transcripts with ELISA data on release after seizure-like activity induced in vitro.

Distinct basal phenotypes of microglia in different regions

We found a distinct basal phenotype, un-related to seizures, for microglia in the CA1/CA3 regions, where few neurons survive in the MTLE-HS syndrome. RNA-seq data from the sclerotic CA1 and CA3 regions was compared to SUB. Microglia of the DG apparently possess an intermediate profile (Blümcke et al, 2007). CA1/CA3 cells tended to an amoeboid, rather than a ramified shape, expressed the activation marker MHCII more strongly and responded to purinergic stimuli more quickly than those in regions with more surviving neurons. Microglial phenotype in the CA1/CA3 regions may be related to a lower neuronal density, rather than to recent neuronal death since triggering events, such as a febrile seizure, occurred in these patients on average 25 years before we obtained the tissue (Supplementary Table 1). An inflammatory environment switches microglial expression of

purinergic receptor subtypes to those promoting retraction rather than extension of cell processes in response to injury (Orr et al., 2009; Gyoneva et al, 2014). Furthermore purinergic stimuli induce changes in the membrane localization of P2RY12 receptors (Dissing-Olesen et al, 2014). Our data showed (Supplementary Figure 6) enhanced numbers of transcripts for the receptors P2RX1, P2RY1, P2RY2 and P2RY13 in sclerotic areas and lower numbers of reads for P2Y14 and the adenosine receptor ADORA2B. Reads for the endonuclease ENTPD2 were higher and those for ENTPD3 lower in sclerotic regions. P2RY1 is associated with microglial migration (De Simone et al, 2010).

The cytokine, IL-10, associated with repair processes (Park et al., 2007), was identified, from the identity of differentially expressed transcripts, as a key regulator of microglial phenotype in the sclerotic CA1/CA3 regions of MTLE-HS tissue. Our data showed IL-10 is more strongly expressed in the CA1/3 region than in SUB (Fig. 4F). Transcriptomic data suggested it is not upregulated and ELISA data suggest it is not secreted after a seizure. Targets of IL-10 include SOCS3 and CD163 which promotes tissue regeneration (Akahori et al., 2015). Our data also predict upregulation of growth factors, including CSF1 and TGFB1 and transcriptional regulators, EPAS1/HIF2A and KLF2, which control epithelial cell development and vascular remodeling (Favier et al., 2001; Novodvorsky and Chico, 2014). Vascular remodeling may be epileptogenic, if integrity of the blood-brain barrier is weakened (van Vliet, Aronica and Gorter, 2014). However IL-10 acts on tight junction proteins to reinforce the barrier (Lin et al., 2018). The functional consequences of such compensation via the upregulation of molecules with regenerative actions, potentially opposed to pro-inflammatory actions, in regions of neuronal loss remain to be clarified. Comparing the vasculature in the glial scar of the CA1/CA3 regions and in the Subiculum would be a first step to define regions of potential regenerative angiogenesis.

The origin of IL-10 remains to be defined. Immunostaining showed it was localized in IBA1+ cells, some of them closely apposed to blood vessels in the CA1 region. Staining with specific markers for infiltrating extracerebral immune cells would help determine if these cells differ from the IBA1+ and P2RY12+ microglia (Mildner et al, 2017), Comparison of the numbers of brain resident microglia with infiltrating T- and B-lymphocytes in MTLE-HS tissue (Ravizza et al., 2008) suggests extracerebral cells have only minor effects on transcriptomic analyses.

A transient secretory phenotype after seizure activity

Pseudotime sorting of RNA-seq data showed a seizure initiates a transient, secretory response. Immunostaining for the seizure markers FOSB and PTGS2 confirmed that effects were local, restricted to one or two regions, in agreement with transcriptomic evidence on cytokine up-regulation. It may well depend on astrocytes (Choi et al., 2014) as well as microglia.

Anatomical, transcriptomic and ELISA data suggest that CXCL8 was the most strongly secreted cytokine. CXCL8 has no rodent homologue (https://www.ncbi.nlm.nih.gov/homologene/47937) and is absent from the Ensembl mouse database (http://www.ensembl.org). It does not figure in reviews of inflammatory targets in epilepsy, based on rodent work (Aronica et al., 2017). However CXCL8 plasma levels increase strongly

after febrile seizures in children (Gallentine et al., 2017) and it is synthesized by human microglia in response to inflammatory stimuli (Ehrlich et al., 1998). In the periphery, CXCL8 is chemotaxic for monocytes and neutrophils (Charo and Ransohoff, 2006), but actions in the brain are poorly defined. After a seizure, we detected CXCL8 at extracellular sites near microglia, presumably in vesicles (Fig. 6H). While the identity of most human and mouse transcripts upregulated after a seizure was congruent, our data (Supplementary material 4) suggests five further human transcripts with no mouse homologue were up-regulated.

Transcripts for the interleukin IL-1B were also strongly increased at short pseudotimes. Transcriptomic and anatomical evidence suggests the NLRP3 inflammasome, a macromolecular complex activated by purinergic stimulation (Di Virgilio et al., 2017) was a key element in IL1B release. The identity of cytokines upregulated in transcriptomic data concurred with ELISA data on secretion after seizure like activity but the profile of release induced by purinergic stimulation was not identical. Cytokine secretion probably does not depend uniquely on purinergic actions on the inflammasome (Lacy and Stow, 2011; Charolidi et al., 2015).

Attention to cytokine secretion after a seizure might improve the management of epileptic patients. Of cytokines identified in this work, IL-1B, IL-6 and TNFA have pro-convulsant actions on GABA and glutamatergic signaling (Stellwagen and Malenka, 2006; Kawasaki et al., 2008) and induce excitotoxic neuronal death (Ye et al., 2013). There is less data on potential epileptogenic effects of CXCL8, but Anakira, an IL-1 receptor antagonist may be a useful therapeutic option as a CXCL8 antagonist (Kenney-Jung et al., 2016). Therapeutic measures against cytokine-related targets could also protect against behavioural disorders linked to seizures. Elevated levels of inflammatory cytokines may degrade human mood, motivation and cognition (Dantzer et al., 2008) and induce depression (Mazarati et al., 2017).

Supplementary Material

Refer to Web version on PubMed Central for supplementary material.

Acknowledgements

We thank Etienne Audinat, Fiona Francis, Gilles Huberfeld, Michel Mallat and Dario Motti for helpful comments, Marie- Agnès Dillies for advice on RNA-seq analysis and Ivan Moszer, Justine Guegan and Vincent Guillemot for help with the PSEA analysis.

Funding:

This work was supported by grants from the European Research Council (322721 ERC-senior), ERAnet Neuron (ANR-12-NEUR-0002-03), Investissements d'Avenir (ANR-10-IAIHU-06) and NeurATRIS (ANR-11-INBS-0011). The École Normale Supérieure genomic platform is supported by the France Génomique infrastructure program and by the Investissements d'Avenir (ANR-10-INBS-09).

Abbreviations

MTLE-HS	mesial temporal lobe epilepsy with hippocampal sclerosis

DG	dentate gyrus
SUB	subiculum

References

Akahori H, Karmali V, Polavarapu R, Lyle AN, Weiss D, Shin E, et al. CD163 interacts with TWEAK to regulate tissue regeneration after ischaemic injury. Nat Commun. 2015; 6 7792.

Amor S, Peferoen LA, Vogel DY, Breur M, van der Valk P, Baker D, et al. Inflammation in neurodegenerative diseases: an update. Immunology. 2014; 142:151–66. [PubMed: 24329535]

Aronica E, Bauer S, Bozzi Y, Caleo M, Dingledine R, Gorter JA, et al. Neuroinflammatory targets and treatments for epilepsy validated in experimental models. Epilepsia. 2017; 58:S27–38.

Avignone E, Lepleux M, Angibaud J, Nägerl UV. Altered morphological dynamics of activated microglia after induction of status epilepticus. J Neuroinflammation. 2015; 12:202. [PubMed: 26538404]

Beach TG, Woodhurst WB, MacDonald DB, Jones MW. Reactive microglia in hippocampal sclerosis associated with human temporal lobe epilepsy. Neurosci Lett. 1995; 191:27–30. [PubMed: 7659283]

Blümcke I, Pauli E, Clusmann H, Schramm J, Becker A, Elger C, et al. A new clinico-pathological classification system for mesial temporal sclerosis. Acta Neuropathol. 2007; 113:235–44. [PubMed: 17221203]

Blümcke I, Thom M, Aronica E, Armstrong DD, Bartolomei F, Bernasconi A, et al. International consensus classification of hippocampal sclerosis in temporal lobe epilepsy: A Task Force report from the ILAE Commission on Diagnostic Methods. Epilepsia. 2013; 54:1315–1329. [PubMed: 23692496]

Boche D, Perry VH, Nicoll JAR. Activation patterns of microglia and their identification in the human brain. Neuropath Appl Neurobiol. 2013; 39:3–18.

Boer K, Spliet WG, van Rijen PC, Redeker S, Troost D, Aronica E. Evidence of activated microglia in focal cortical dysplasia. J Neuroimmunol. 2006; 173:188–95. [PubMed: 16483671]

Bohlen CJ, Bennett FC, Tucker AF, Collins HY, Mulinyawe SB, Barres BA. Diverse Requirements for Microglial Survival, Specification, and Function Revealed by Defined-Medium Cultures. Neuron. 2017; 94:759–773. [PubMed: 28521131]

Bryan NB, Dorfleutner A, Rojanasakul Y, Stehlik C. Activation of inflammasomes requires intracellular redistribution of the apoptotic speck-like protein containing a caspase recruitment domain. Immunol. 2009; 182:3173–82.

Butovsky O, Jedrychowski MP, Moore CS, Cialic R, Lanser AJ, Gabriely G, et al. Identification of a unique TGF-β-dependent molecular and functional signature in microglia. Nat Neurosci. 2014; 17(1):131–43. [PubMed: 24316888]

Carow B, Rottenberg ME. SOCS3, a Major Regulator of Infection and Inflammation. Front Immunol. 2014; 5:58. [PubMed: 24600449]

Charo IF, Ransohoff RM. The Many Roles of Chemokines and Chemokine Receptors in Inflammation. N Engl J Med. 2006; 354:610–621. [PubMed: 16467548]

Charolidi N, Schilling T, Eder C. Microglial Kv1.3 Channels and P2Y12 receptors differentially regulate cytokine and chemokine release from brain slices of young adult and aged mice. PLoS One. 2015; 10:e0128463. [PubMed: 26011191]

Chiavegato A, Zurolo E, Losi G, Aronica E, Carmignoto G. The inflammatory molecules IL-1β and HMGB1 can rapidly enhance focal seizure generation in a brain slice model of temporal lobe epilepsy. Front Cell Neurosci. 2014 Jun 6.8:155. [PubMed: 24936172]

Choi SS, Lee HJ, Lim I, Satoh J, Kim SU. Human astrocytes: secretome profiles of cytokines and chemokines. PLoS One. 2014; 9:e92325. [PubMed: 24691121]

Cook MJ, O'Brien TJ, Berkovic SF, Murphy M, Morokoff A, Fabinyi G, et al. Prediction of seizure likelihood with a long-term, implanted seizure advisory system in patients with drug-resistant epilepsy: A first-in-man study. Lancet Neurol. 2013; 12:563–571. [PubMed: 23642342]

Europe PMC Funders Author Manuscripts

Europe PMC Funders Author Manuscripts

Crespel A, Coubes P, Rousset MC, Brana C, Rougier A, Rondouin G, et al. Inflammatory reactions in human medial temporal lobe epilepsy with hippocampal sclerosis. Brain Res. 2002; 952:159–69. [PubMed: 12376176]

Dantzer R, O'Connor JC, Freund GG, Johnson RW, Kelley KW. From inflammation to sickness and depression: when the immune system subjugates the brain. Nat Rev Neurosci. 2008; 9:46–56. [PubMed: 18073775]

Davalos D, Grutzendler J, Yang G, Kim JV, Zuo Y, Jung S, et al. ATP mediates rapid microglial response to local brain injury in vivo. Nat Neurosci. 2005; 8:752–758. [PubMed: 15895084]

De Simone R, Niturad CE, De Nuccio C, Ajmone-Cat MA, Visentin S, Minghetti L. TGF-β and LPS modulate ADP-induced migration of microglial cells through P2Y1 and P2Y12 receptor expression. J Neurochem. 2010; 115(2):450–9. [PubMed: 20681951]

Dissing-Olesen L, LeDue JM, Rungta RL, Hefendehl JK, Choi HB, MacVicar BA. Activation of neuronal NMDA receptors triggers transient ATP-mediated microglial process outgrowth. J Neurosci. 2014 Aug 6; 34(32):10511–27. [PubMed: 25100586]

Di Virgilio F, Dal Ben D, Sarti AC, Giuliani AL, Falzoni S. The P2X7 Receptor in Infection and Inflammation. Immunity. 2017; 47:15–31. [PubMed: 28723547]

Ehrlich LC, Hu S, Sheng WS, Sutton RL, Rockswold GL, Peterson PK, et al. Cytokine regulation of human microglial cell IL-8 production. J Immunol. 1998; 160:1944–8. [PubMed: 9469457]

Favier J, Kempf H, Corvol P, Gasc JM. Coexpression of endothelial PAS protein 1 with essential angiogenic factors suggests its involvement in human vascular development. Dev Dyn. 2001; 222:377–88. [PubMed: 11747073]

Franceschini A, Capece M, Chiozzi P, Falzoni S, Sanz JM, Sarti AC, et al. The P2X7 receptor directly interacts with the NLRP3 inflammasome scaffold protein. FASEB J. 2015; 29:2450–61. [PubMed: 25690658]

Galatro TF, Holtman IR, Lerario AM, Vainchtein ID, Brouwer N, Sola P, et al. Transcriptomic analysis of purified human cortical microglia reveals age-associated changes. Nat Neurosci. 2017; 20:1162–1171. [PubMed: 28671693]

Gallentine WB, Shinnar S, Hesdorffer DC, Epstein L, Nordli DR, Lewis DV, et al. Plasma cytokines associated with febrile status epilepticus in children: A potential biomarker for acute hippocampal injury. Epilepsia. 2017; 58:1102–1111. [PubMed: 28448686]

Gorter JA, van Vliet EA, Aronica E. Status epilepticus, blood-brain barrier disruption, inflammation, and epileptogenesis. Epilepsy Behav. 2015; 49:13–6. [PubMed: 25958228]

Gyoneva S, Davalos D, Biswas D, Swanger SA, Garnier-Amblard E, Loth F, et al. Systemic inflammation regulates microglial response to tissue damage in vivo. Glia. 2014; 62:1345–60. [PubMed: 24807189]

Huberfeld G, Menendez de la Prida L, Pallud J, Cohen I, Le Van Quyen M, Adam C, et al. Glutamatergic pre-ictal discharges emerge at the transition to seizure in human epilepsy. Nat Neurosci. 2011; 14:627–34. [PubMed: 21460834]

Irani SR, Bien CG, Lang B. Autoimmune epilepsies. Curr Opin Neurol. 2011; 24:146–53. [PubMed: 21358545]

Jimenez-Pacheco A, Diaz-Hernandez M, Arribas-Blázquez M, Sanz-Rodriguez A, Olivos-Oré LA, Artalejo AR, et al. Transient P2X7 Receptor Antagonism Produces Lasting Reductions in Spontaneous Seizures and Gliosis in Experimental Temporal Lobe Epilepsy. J Neurosci. 2016; 25(22):5920–32.

Jourdren L, Bernard M, Dillies MA, Le Crom S. Eoulsan: A cloud computing-based framework facilitating high throughput sequencing analyses. Bioinformatics. 2012; 28:1542–1543. [PubMed: 22492314]

Kawasaki Y, Zhang L, Cheng J-K, Ji R-R. Cytokine mechanisms of central sensitization: distinct and overlapping role of interleukin-1beta, interleukin-6, and tumor necrosis factor-alpha in regulating synaptic and neuronal activity in the superficial spinal cord. J Neurosci. 2008; 8:5189–94.

Kenney-Jung DL, Vezzani A, Kahoud RJ, LaFrance-Corey RG, Ho ML, et al. Febrile infection-related epilepsy syndrome treated with anakinra. Ann Neurol. 2016; 80:939–945. [PubMed: 27770579]

Kettenmann H, Hanisch U-K, Noda M, Verkhratsky A. Physiology of Microglia. Physiol Rev. 2011; 91:461–553. [PubMed: 21527731]

Koizumi S, Shigemoto-Mogami Y, Nasu-Tada K, Shinozaki Y, Ohsawa K, Tsuda M, et al. UDP acting at P2Y6 receptors is a mediator of microglial phagocytosis. Nature. 2007; 446:1091–1095. [PubMed: 17410128]

Koscsó B, Csóka B, Selmeczy Z, Himer L, Pacher P, Virág L, et al. Adenosine augments IL-10 production by microglial cells through an A2B adenosine receptor-mediated process. J immunol. 2012; 188(1):445–53. [PubMed: 22116830]

Koscsó B, Csóka B, Kókai E, Németh ZH, Pacher P, Virág L, et al. Adenosine augments IL-10-induced STAT3 signaling in M2c macrophages. J Leukoc Biol. 2013; 94(6):1309–15. [PubMed: 23922379]

Kuhn A, Thu D, Waldvogel HJ, Faull RLM, Luthi-Carter R. Population-specific expression analysis (PSEA) reveals molecular changes in diseased brain. Nat Methods. 2011; 8:945–947. [PubMed: 21983921]

Kumaria A, Tolias CM, Burnstock G. ATP signalling in epilepsy. Purinergic Signalling. 2008; 4:339–346. [PubMed: 18568425]

Lacar B, Linker SB, Jaeger BN, Krishnaswami S, Barron J, Kelder M, et al. Nuclear RNA-seq of single neurons reveals molecular signatures of activation. Nat Commun. 2016; 7 11022.

Lacy P, Stow JL. Cytokine release from innate immune cells: association with diverse membrane trafficking pathways. Blood. 2011; 118:9–18. [PubMed: 21562044]

Latz E, Xiao TS, Stutz A. Activation and regulation of the inflammasomes. Nat Rev Immunol. 2013; 13:397–411. [PubMed: 23702978]

Leal B, Chaves J, Carvalho C, Rangel R, Santos A, Bettencourt A, et al. Brain expression of inflammatory mediators in Mesial Temporal Lobe Epilepsy patients. J Neuroimmunol. 2017; 313:82–88. [PubMed: 29153613]

Lerner-Natoli M, Montpied P, Rousset MC, Bockaert J, Rondouin G. Sequential expression of surface antigens and transcription factor NFκB by hippocampal cells in excitotoxicity and experimental epilepsy. Epilepsy Res. 2000; 41:141–154. [PubMed: 10940615]

Li H, Handsaker B, Wysoker A, Fennell T, Ruan J, Homer N, Marth G, Abecasis G, Durbin R, 1000 Genome Project Data Processing Subgroup. The Sequence Alignment/Map format and SAMtools. Bioinformatics. 2009; 25:2078–2079. [PubMed: 19505943]

Lin R, Chen F, Wen S, Teng T, Pan Y, Huang H. Interleukin-10 attenuates impairment of the blood-brain barrier in a severe acute pancreatitis rat model. J Inflamm. 2018; 27:15–4.

Louboutin J-P, Strayer DS. Relationship between the chemokine receptor CCR5 and microglia in neurological disorders: consequences of targeting CCR5 on neuroinflammation, neuronal death and regeneration in a model of epilepsy. CNS Neurol Disord Drug Targets. 2013; 12:815–29. [PubMed: 24047524]

Love MI, Huber W, Anders S. Moderated estimation of fold change and dispersion for RNA-seq data with DESeq2. Genome Biol. 2014; 15:550. [PubMed: 25516281]

Mazarati AM, Lewis ML, Pittman QJ. Neurobehavioral comorbidities of epilepsy: Role of inflammation. Epilepsia. 2017; 58:48–56. [PubMed: 28675557]

Mildner A, Huang H, Radke J, Stenzel W, Priller J. P2Y12 receptor is expressed on human microglia under physiological conditions throughout development and is sensitive to neuroinflammatory diseases. Glia. 2017; 65:375–387. [PubMed: 27862351]

Nash B, Meucci O. Functions of the Chemokine Receptor CXCR4 in the Central Nervous System and Its Regulation by μ-Opioid Receptors. Int Rev Neurobiol. 2014; 118:105–128. [PubMed: 25175863]

Novodvorsky P, Chico TJ. The role of the transcription factor KLF2 in vascular development and disease. Prog Mol Biol Transl Sci. 2014; 124:155–88. [PubMed: 24751430]

Orr AG, Orr AL, Li X-J, Gross RE, Traynelis SF. Adenosine A2A receptor mediates microglial process retraction. Nat Neurosci. 2009; 12:872–878. [PubMed: 19525944]

Park KW, Lee HG, Jin BK, Lee YB. Interleukin-10 endogenously expressed in microglia prevents lipopolysaccharide-induced neurodegeneration in the rat cerebral cortex in vivo. Exp Mol Med. 2007; 39:812–9. [PubMed: 18160852]

Pernhorst K, Herms S, Hoffmann P, Cichon S, Schulz H, Sander T, et al. TLR4, ATF-3 and IL8 inflammation mediator expression correlates with seizure frequency in human epileptic brain tissue. Seizure. 2013; 22:675–678. [PubMed: 23706953]

Peruzzotti-Jametti L, Donegá M, Giusto E, Mallucci G, Marchetti B, Pluchino S. The role of the immune system in central nervous system plasticity after acute injury. Neuroscience. 2014; 283:210–221. [PubMed: 24785677]

Popkirov S, Ismail FS, Grönheit W, Kapauer M, Wellmer J, Bien CG. Progressive hippocampal sclerosis after viral encephalitis: Potential role of NMDA receptor antibodies. Seizure. 2017; 51:6–8. [PubMed: 28750305]

Ravizza T, Gagliardi B, Noé F, Boer K, Aronica E, Vezzani A. Innate and adaptive immunity during epileptogenesis and spontaneous seizures: Evidence from experimental models and human temporal lobe epilepsy. Neurobiol Dis. 2008; 29:142–160. [PubMed: 17931873]

Réu P, Khosravi A, Bernard S, Mold JE, Salehpour M, Alkass K, et al. The Lifespan and Turnover of Microglia in the Human Brain. Cell Rep. 2017; 20:779–784. [PubMed: 28746864]

Rigau V, Morin M, Rousset MC, de Bock F, Lebrun A, Coubes P, et al. Angiogenesis is associated with blood-brain barrier permeability in temporal lobe epilepsy. Brain. 2007; 130:1942–56. [PubMed: 17533168]

Ryan MM, Mason-Parker SE, Tate WP, Abraham WC, Williams JM. Rapidly induced gene networks following induction of long-term potentiation at perforant path synapses in vivo. Hippocampus. 2011; 21:541–53. [PubMed: 20108223]

Saraiva M, O'Garra A. The regulation of IL-10 production by immune cells. Nat Rev Immunol. 2010; 10:170–181. [PubMed: 20154735]

Schwendele B, Brawek B, Hermes M, Garaschuk O. High-resolution in vivo imaging of microglia using a versatile nongenetically encoded marker. Eur J Immunol. 2012; 42:2193–6. [PubMed: 22622946]

Stellwagen D, Malenka RC. Synaptic scaling mediated by glial TNF-α. Nature. 2006; 440:1054–1059. [PubMed: 16547515]

Trapnell C, Cacchiarelli D, Grimsby J, Pokharel P, Li S, Morse M, et al. The dynamics and regulators of cell fate decisions are revealed by pseudotemporal ordering of single cells. Nat Biotechnol. 2014; 32:381–386. [PubMed: 24658644]

Vezzani A, Conti M, De Luigi A, Ravizza T, Moneta D, Marchesi F, et al. Interleukin-1beta immunoreactivity and microglia are enhanced in the rat hippocampus by focal kainate application: functional evidence for enhancement of electrographic seizures. J Neurosci. 1999; 19:5054–65. [PubMed: 10366638]

Vezzani A, Friedman A, Dingledine RJ. The role of inflammation in epileptogenesis. Neuropharm. 2013; 69:16–24.

van Vliet EA, Aronica E, Gorter JA. Role of blood-brain barrier in temporal lobe epilepsy and pharmacoresistance. Neuroscience. 2014; 277:455–73. [PubMed: 25080160]

Virta M, Hurme M, Helminen M. Increased plasma levels of pro- and anti-inflammatory cytokines in patients with febrile seizures. Epilepsia. 2002; 43:920–923. [PubMed: 12181012]

Ye L, Huang Y, Zhao L, Li Y, Sun L, Zhou Y, et al. IL-1β and TNFα induce neurotoxicity through glutamate production: A potential role for neuronal glutaminase. J Neurochem. 2013; 125:897–908. [PubMed: 23578284]

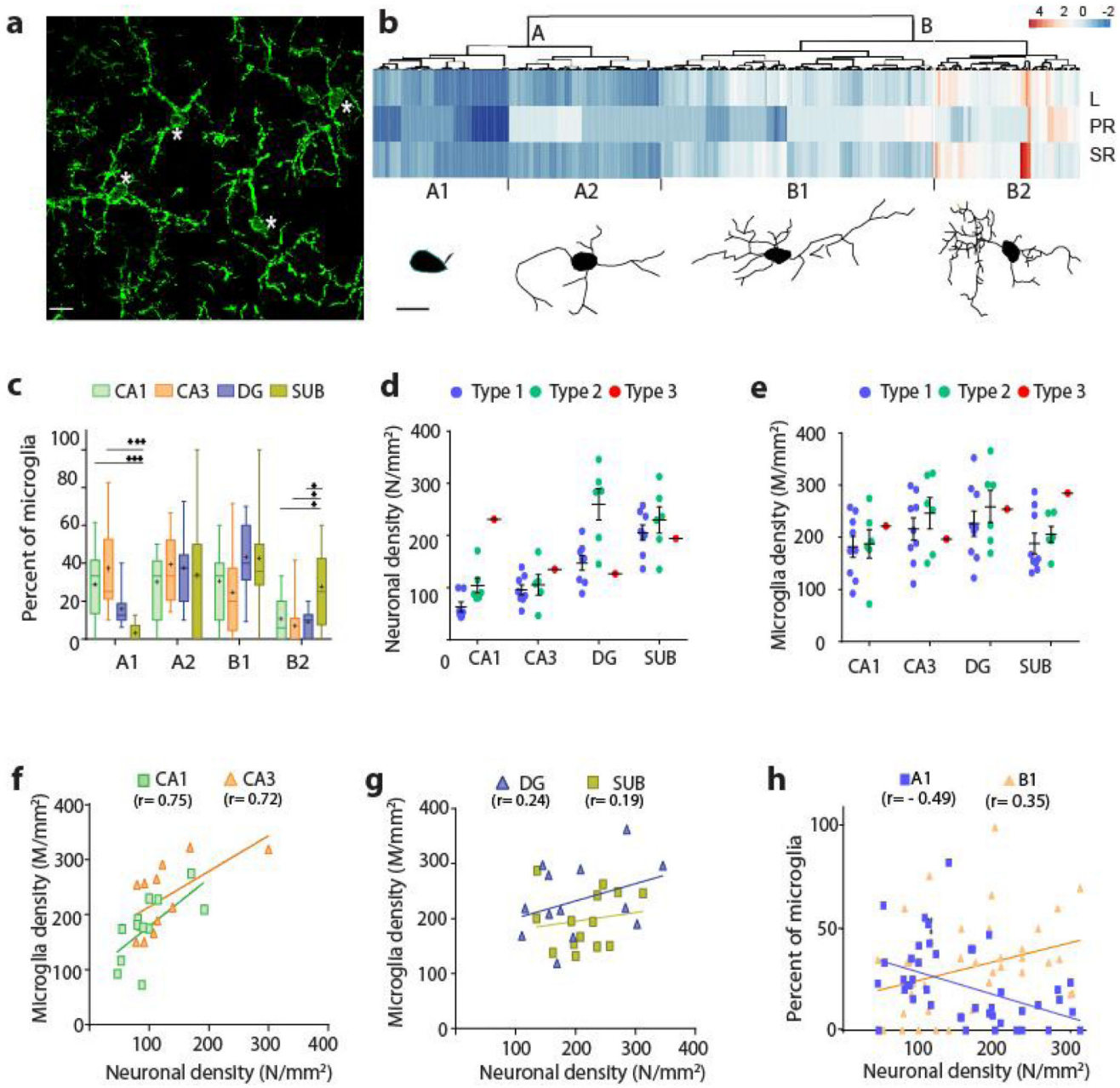

Figure 1. Diverse microglia shape and distribution.

(A) Diverse forms (stars) of IBA1+ microglia in the DG. (B) Cluster analysis of microglia shape (n=283 from CA1, CA3, SUB and DG of 9 patients) based on total length, L, number of primary ramifications, PR, and secondary ramifications, SR. Unsupervised clustering (Euclidean distance, Ward method) separated produced four groups, A1, A2, B1 and B2. The scale bar indicates normalized values for L, PR and SR. A typical reconstructed cell of each cluster is shown below. Scale bar: 10μm. (C) Interleaved box and whiskers plot showing the minimum and maximum % of microglia in clusters A1-B2 in CA1, CA3, DG and Sub. Differences were significant at $p<0.005$ (***) or $p=0.05$ (*), 2-way ANOVA with

Europe PMC Funders Author Manuscripts

Tukey's multiple comparison. Lines show a mean of 30 microglia per patient (n=15). (D) Neuronal and (E) microglia densities (cells/mm^2) in CA1, CA3, DG and Sub (n=13 patients). The type of hippocampal sclerosis was 1, blue; 2, green or 3, red. Bar is mean ± SEM. (F) Microglia and neuronal densities were well correlated in CA1 (r=0.75 p=0.006, n=12 patients) and CA3 (r=0.72, p=0.001, n=12 patients) but less well correlated (G) in DG (r=0.24, p=0.4, n=13 patients) and SUB (r=0.19, p=0.5, n=14 patients).Spearman correlation, two tailed p-value. (H) Amoeboid microglia of cluster A1 (blue) were associated with regions of low neuronal density (r=-0.49, p=0.006, n=44; Spearman correlation) and ramified cells (cluster B1) with regions of higher neuronal density (r=-0.35, p=0.01, n=44; Spearman correlation, 2-tailed p).

Europe PMC Funders Author Manuscripts

Europe PMC Funders Author Manuscripts

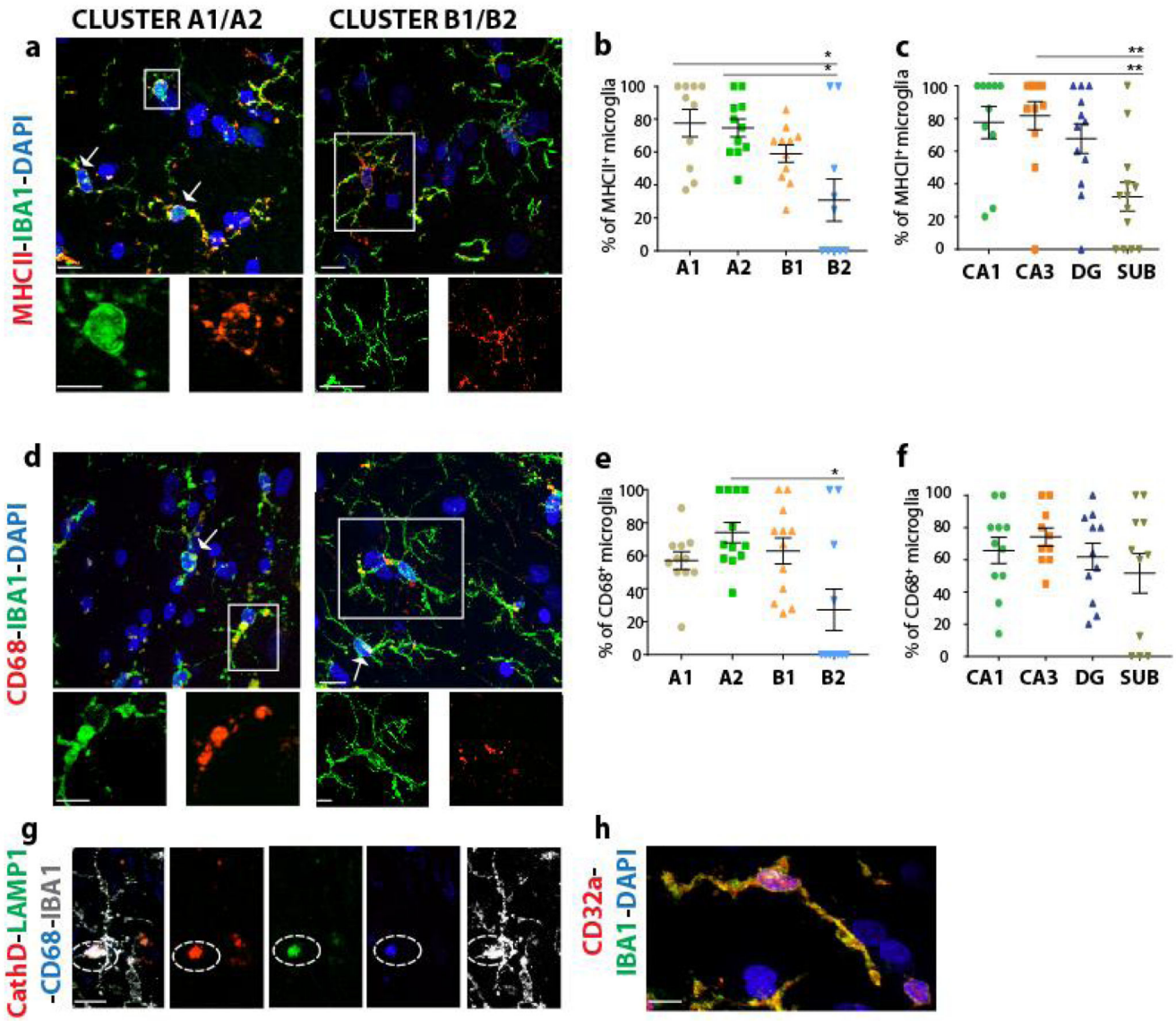

Figure 2. Correlation of microglia phenotype marker with differences in form.

(A) Immunostaining for MHCII (purple) in microglia of clusters A1/A2 and B1/B2. Counterstained for IBA1+ (green) and DAPI (blue). Insets below, show MHCII+ in soma (A1/A2) or processes (B1/B2). Scale 10 μm. (B) Density of MCHII+ microglia for cells of clusters A1, A2, B1 and B2 and for (C) cells of the CA1, CA3, DG and subicular regions. Each point is a mean of 15 microglia (n=10 or 11 patients). Bar is ± SEM. (D) Immunostaining for CD68 (purple) in microglia, counterstained for IBA1 (green) and DAPI (blue) of clusters A1/A2 and B1/B2. Insets below, show CD68+ vesicles in microglia processes. Scale 10μm, 5μm for inset. (E) Density of CD68+ microglia for cells of clusters A1, A2, B1 and B2 and for (F) cells of the CA1, CA3, DG and subiculum. Fewer microglia of cluster B2 were CD68+, but little difference between regions. Each point is a mean of 15 microglia (n=10 or 11 patients). Bar shows mean +/- SEM. No significant differences were evident between areas. (G) Immunostaining shows CD68 (blue), Lamp1 (green), and

Cathepsin D (red) colocalization in the phago-lysosome of an IBA1+ microglia (white). Scale bar 10μm. (H) CD32a (purple) staining, with IBA1 (green) and DAPI (blue) counterstain confirms the phagocytic phenotype. Scale bar 10μm. Stars in B, C, E, F show significance (Mann-Whitney 2-tailed test at $p<0.01$, ** and at $p<0.05$, *).

Europe PMC Funders Author Manuscripts

Europe PMC Funders Author Manuscripts

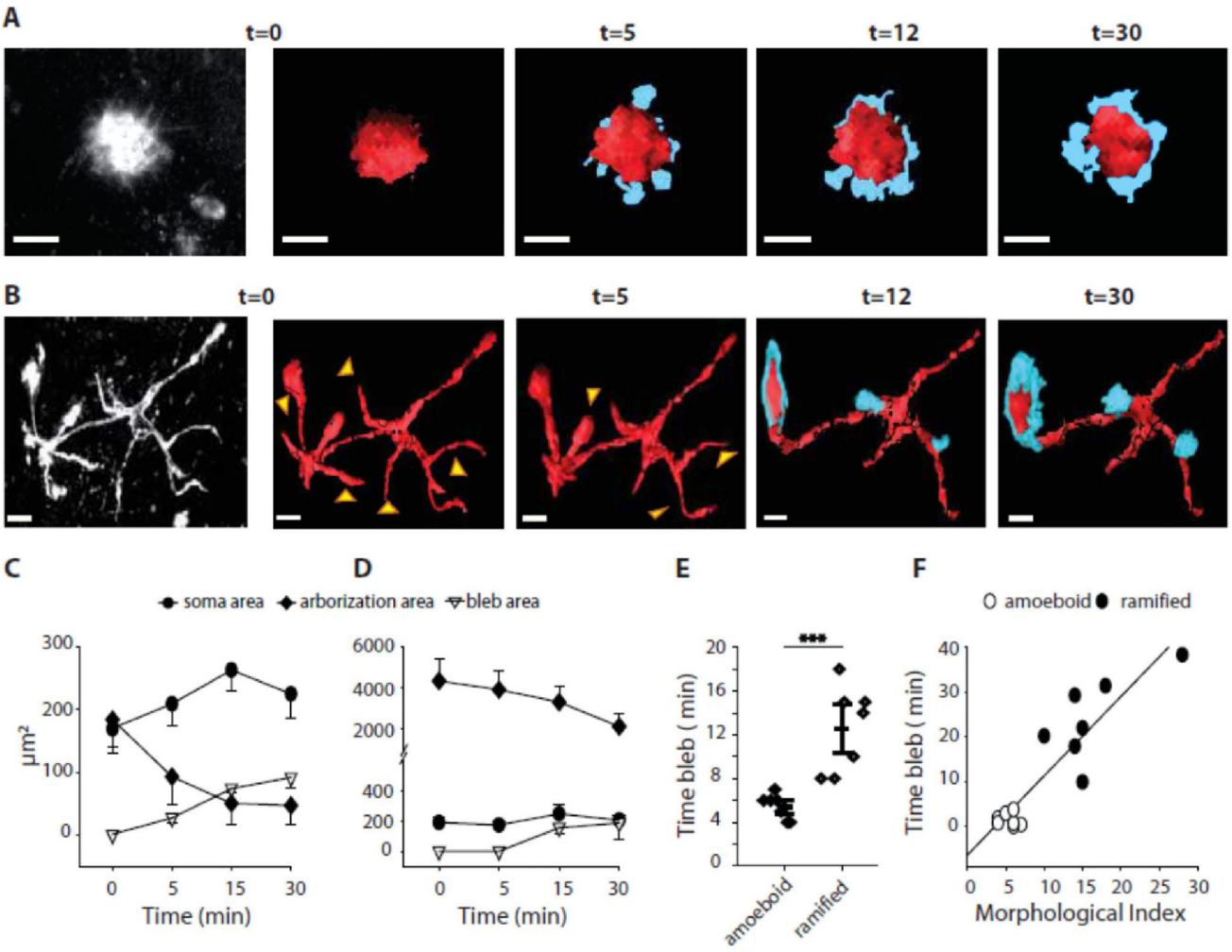

Figure 3. Microglia of different shapes respond differently to purinergic stimuli.

(A) changes in form of an amoeboid microglia from the CA1 region and (B) a ramified microglia of the subiculum induced by 2 mM ADP. Two-photon imaging of cells stained with a fluorescent tomato lectin. At left, a microglia imaged at t=0 and towards the right 3D reconstructions from t=0, 5, 12, 30 min after ADP stimulus onset. Scale bar 10µm. Light blue in 3D images, differences between successive reconstructions, shows ruffling of amoeboid and ramified cells. Yellow arrows for ramified microglia point to process retraction between 0 and 5, and between 5 and 12 min. (C) Time course of changes in mean somatic area (circles), arborization area (diamonds) and bleb area (triangles) for amoeboid microglia (n=7, 3 patients) and for (D) ramified microglia (n=7, 2 patients). (E) A longer delay from ADP application to membrane ruffling for ramified than for amoeboid microglia (2-tailed t test, t = -4,554 -, p< 0.001, n=14, 5 patients). (F) Correlation between cellular morphological index and the latency to ruffling. (Pearson correlation, r = 0.9; p=9.0e^{-6}). Amoeboid microglia open circles, ramified microglia filled circles.

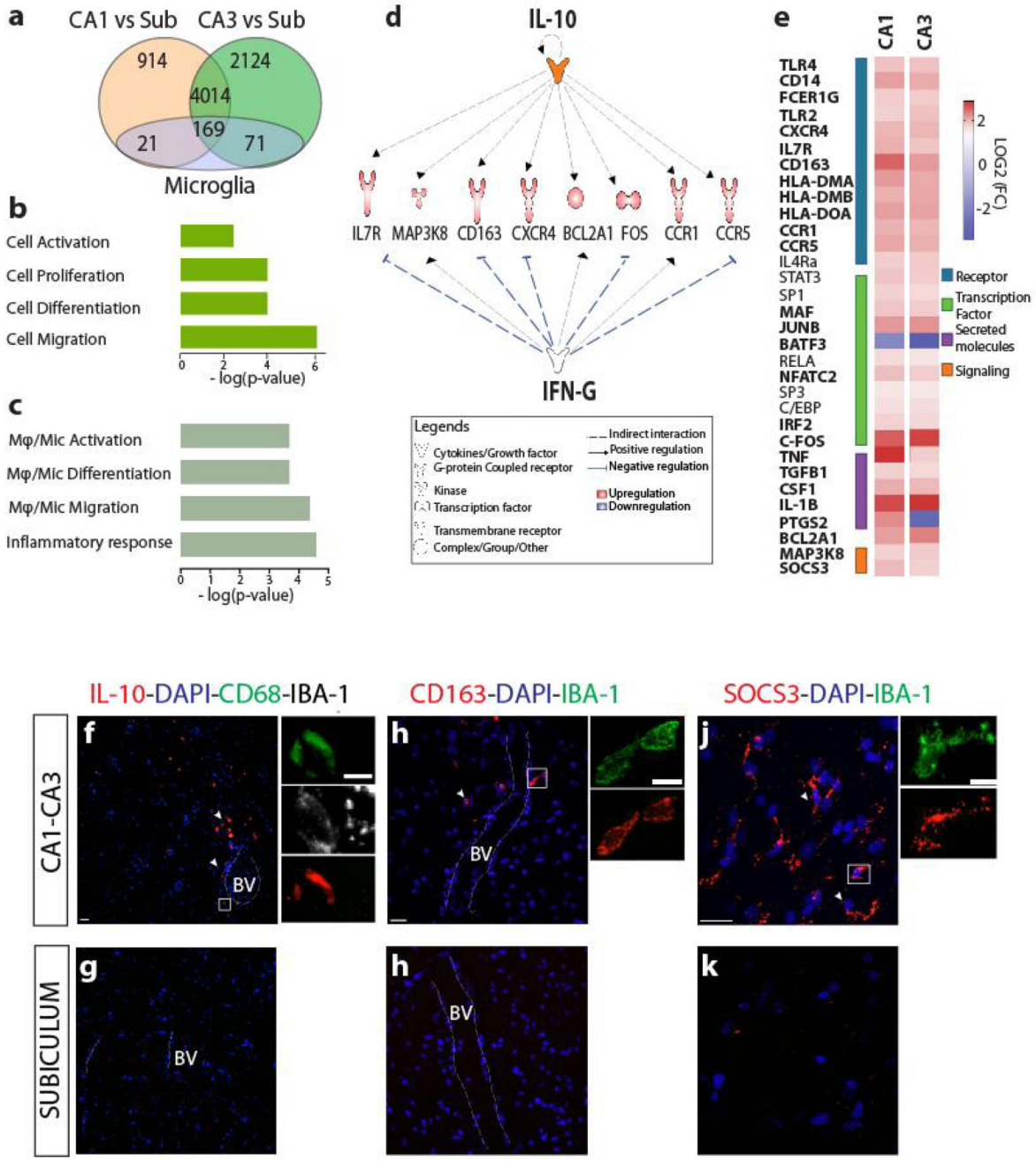

Figure 4. Transcriptomic profile for regions of high or low neuronal death.

(A) Venn diagram of transcripts differentially expressed between CA1 or CA2/CA3 and SUB (n=7313, tissue from 12 patients, not including the type III sclerosis tissue, p-adj < 0.05). 169 microglia associated transcripts were differentially expressed. (B) Top five enriched cellular functions (IPA analysis; -log(p-value); z-score>2) deduced from all differentially expressed transcripts. (C) Top 5 enriched functions (–log p-value) from microglia associated transcripts (PSEA, Supplementary material 2). (D) Predicted network of links to cytokine regulators (IPA). The anti-inflammatory cytokine IL-10 was predicted

Europe PMC Funders Author Manuscripts

from transcripts upregulated in CA1 and CA3. IL-10 acts inversely to the cytokine IFNG on 5 out of 7 downstream molecules (direct effect, solid line; z-score>2). Significant upregulation, red; activation of regulators, orange (z-score>2). (E) Heatmap of log2 fold changes for differentially regulated and IL-10 related, transcripts (p-adj <0.05). Microglia-associated in bold. (F) IL-10 (purple) is more highly expressed in CA1-CA3 than in SUB. Insets right, immunostaining for IL- 10 (purple), IBA1+ (white) and CD68 (green). (G) CD163 (red) immunostaining near blood vessels (BV) in CA1-3, but not SUB. Inset right CD163 staining (purple) in IBA1+ cell (green). (H) SOCS3 (purple) is more strongly expressed in IBA1+ (green) cells of CA1-3 than SUB. Inset right, SOCS3 signal in IBA1+ microglia. Scale bar 10μm. DAPI (blue) nuclear counterstain.

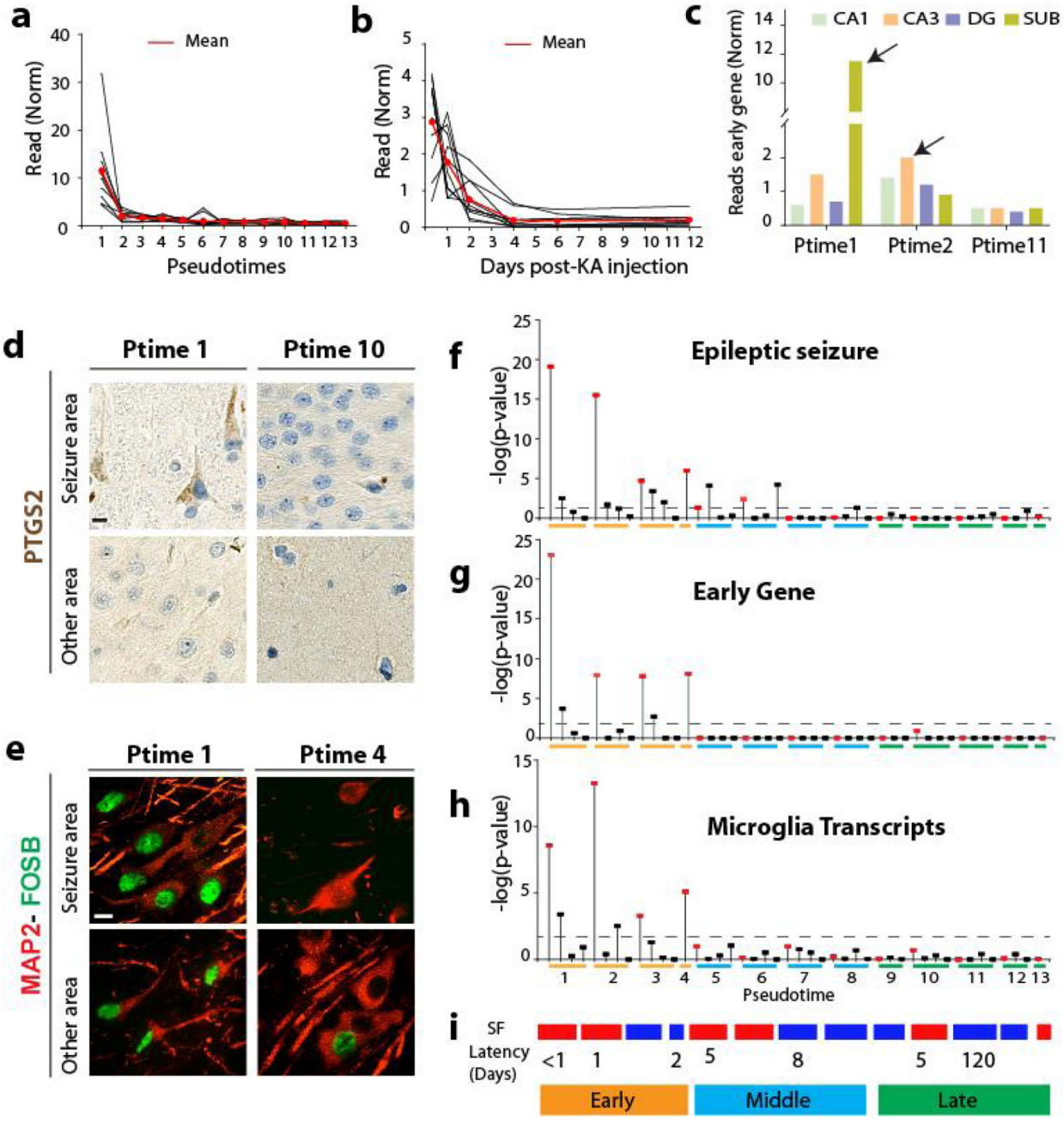

Figure 5. Transcriptomic and anatomical evidence for a recent, local seizure

(A) Ordered reads for immediate early genes (ARC, EGR1, FOS, FOSB, FOSL1, IER2, JUN, JUNB, NR4A1 and NR4A3) in tissue from 13 patients. Mean of 10 (red line) and values for each transcript (black lines). Highest value from any area (CA1, CA3, DG, SUB) is shown for each patient. Reads from all transcripts normalized to 1 over all samples. (B) Mean reads for the same immediate early genes in mouse CA1 region tissue at defined delays after kainic-acid (KA) treatment. Transcript differences between KA (n=3) or NaCl (n=3) injected animals at 6 hrs to 12 days after KA-injection. Red line mean of 10

Europe PMC Funders Author Manuscripts

transcripts. (C) Variation in mean reads for 10 immediate early genes from CA1, CA3, DG and SUB region of patients ordered to ptimes1, 2 and 11. The region (arrow) with the highest mean value of immediate early gene reads was defined as seizure-associated area for ptimes 1 and 2. (D) Immunostaining for PTGS2 (brown) in a seizure-associated and a non-seizure associated region at ptime1 tissue and ptime10 tissue. Scale, 20μm. (E) Immunostaining for MAP2 (purple) and Fos B (green) in seizure-associated and non-seizure associated regions from ptime1 and ptime4 tissue. Scale, 20μm. (Fi-iv) Data from all samples: 13 patients, ptimes1–13, 1-4 regions per patient, seizure-associated regions in red. Significance at p=0.05, dotted line. (Fi) –log p-values for enrichment of the function 'epileptic seizure' (IPA, 190 transcripts) from each sample (log2FC > ±1.5, p-adj<0.05), red point is the seizure-associated area. (Fii) -log p-value for differential expression of the 10 immediate early genes (Fiii) -log p-value for transcripts enriched in microglia (623 transcripts, PSEA list). (Fiv) Patients 1-13. High reported seizure frequency, red; low reported seizure frequency, blue. Numbers are clinical estimates of the latency from the last seizure to tissue collection

Europe PMC Funders Author Manuscripts

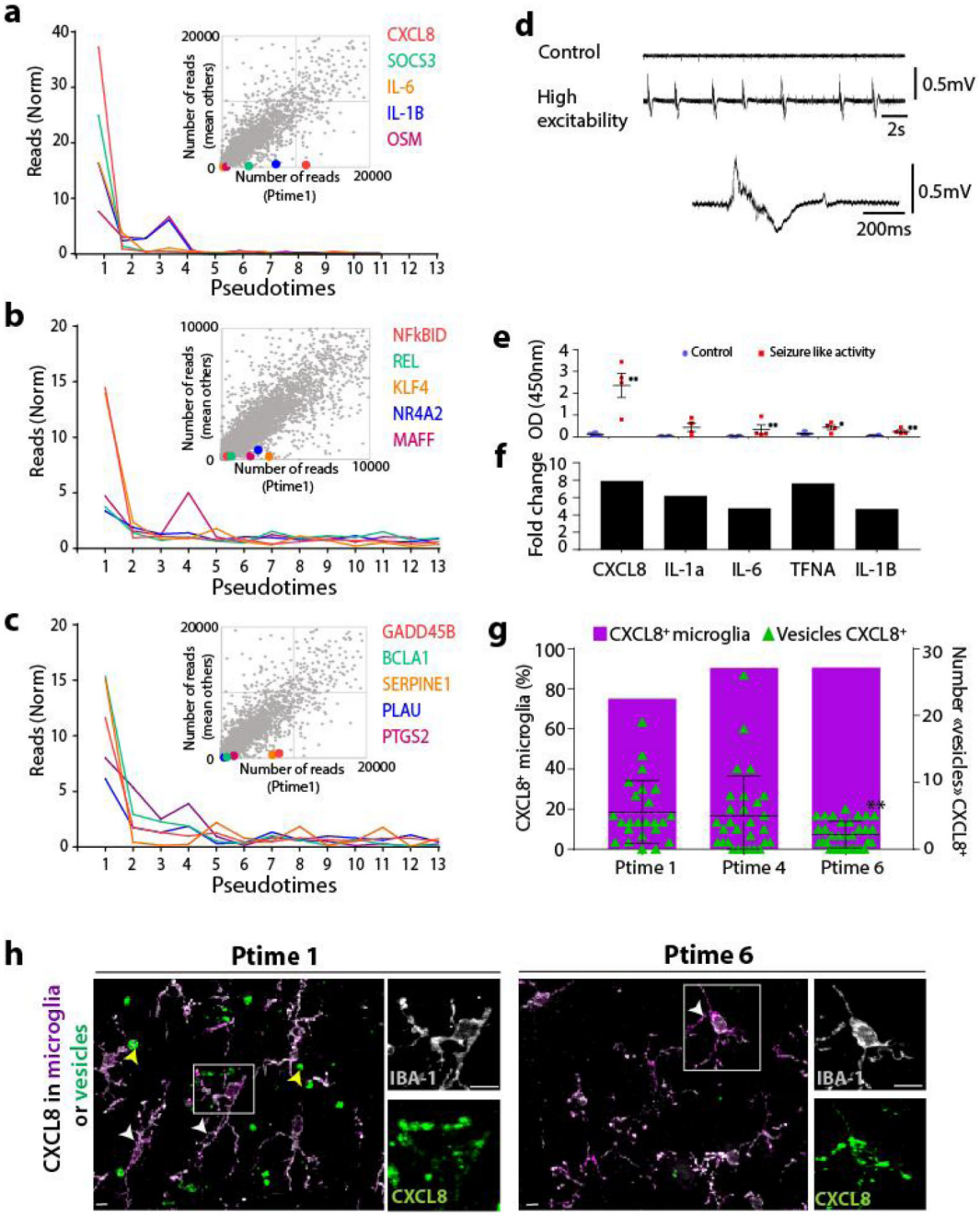

Figure 6. Pseudotime kinetics of the response to a seizure.

(A) variation in the top 5 reads for cytokine-related transcripts, (B) immune-related transcription factors and for (C) other molecules from ptimes1 -13. Values for the seizure-associated region of each patient. Each inset highlights the top 5 transcripts on plots of reads of all transcripts from the seizure-associated region at ptime1 against mean reads for all other samples. (D) Field records of seizure-like activity generated by a naïve human temporal lobe slice (unknown delay from last seizure) exposed to high excitability solution. (E) Cytokine release (CXCL8, IL-1A, IL-6, TFNA and IL-1B, multiplex-ELISA) from

superfusate of acute slice after seizure-like activity (red) or after exposure to a control solution (blue). Bars show mean ± SEM. Stars, differences significant at ** $p<0.01$, or at * $p<0.05$ (n=4-6 patients, Mann-Whitney, 2-tailed p-value). (F) Fold enrichment of reads for the same cytokines in the seizure-associated area (defined from immediate early genes) at ptime1 compared to ptimes5-13 (all areas, all patients). (G) Changes in the proportion of CXCL8 immunopositive microglia (purple), numbers of extracellular CXCL8+ vesicles at less than 10μm from IBA1+ microglia (green) for ptimes1, 4 and 6. Stars show differences significant at **$p<0.01$ - (n=25-30 cells per patient, Mann Whitney, 2-tailed p-value). (H) CXCL8 (green) and IBA1 (white) immunostaining in tissue from ptimes1 and 6. Purple indicates CXCL8 colocalization with IBA1 (white arrow). Green shows extracellular CXCL8 vesicles (yellow arrow). Insets show co-localization at higher resolution. CXCL8+ microglia increased from ptime1-6. Extracellular CXCL8+ vesicles were detected only at ptimes1-4. Scale bar, 10μm.

Europe PMC Funders Author Manuscripts

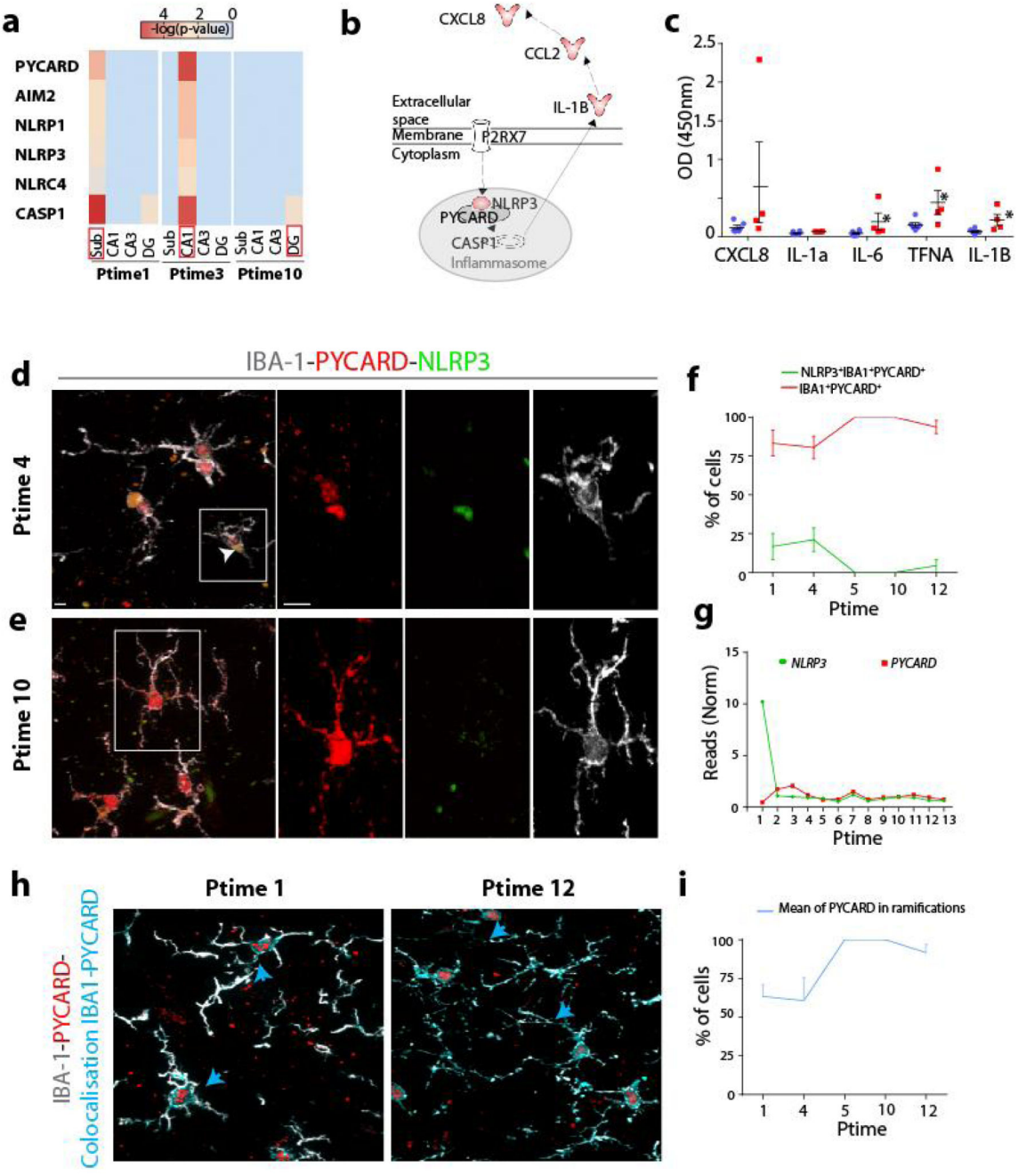

Figure 7. NLRP3 inflammasome and cytokine secretion.

(A) Inflammasome linked transcripts predicted as key regulators in seizure-associated tissue at ptimes1-4. Heatmap of –log (p-value) for inflammasome components in seizure-associated regions (red box) at ptimes1, 3 and 10. (B) Pathway for P2RX7 receptor, inflammasome activation and cytokine secretion (from IPA). Upregulated transcripts from ptimes1-4, red. (C) Cytokine secretion (multiplex-ELISA) from superfusate of temporal lobe slices exposed to 2 mM ADP (red) or control solution (blue). Stars show differences significant at * $p<0.05$ (n=4-6, Mann-Whitney, 2-tailed p-value). (D) Immuno-staining for

NLRP3 (green) and PYCARD (purple) inflammasome components in IBA1+ cells (blue) of tissue from ptime4 and (F) ptime 10. NLRP3 and PYCARD colocalize in microglia at ptime4 but not ptime10. Scale bar 10μm. (E) Proportion of microglia expressing NLRP3 and PYCARD (green) or only PYCARD (purple) at ptime1, 4, 5, 10 and 12 (mean ± SEM for 20 microglia per patient in all areas). PYCARD was present at all ptimes, but colocalized with NLRP3 only at ptimes1-4 when (G) reads for NLRP3 were elevated. (H) Immunostaining of PYCARD (Red) and IBA1 (white) at ptime1 and (G) ptime12. Blue indicates IBA1 and PYCARD colocalization (Blue arrow). (I) As perisomatic NLRP3 was reduced, PYCARD migrated to microglia ramifications. Data from 20 microglia at ptimes 1–12.